Hindawi
Complexity
Volume 2018, Article ID 4920750, 9 pages
https://doi.org/10.1155/2018/4920750

Research Article

Exploration of Muscle Fatigue Effects in Bioinspired Robot Learning from sEMG Signals

Ning Wang[1,2] **Yang Xu**[3] **Hongbin Ma**[4] **and Xiaofeng Liu**[5,6,7]

[1]*School of Computing, Electronics and Mathematics, Plymouth University, Drake Circus, Plymouth PL4 8AA, UK*
[2]*Shenzhen Research Institute, The Chinese University of Hong Kong, Shatin, Hong Kong*
[3]*Key Laboratory of Autonomous Systems and Networked Control, College of Automation Science and Engineering, South China University of Technology, Guangzhou 510640, China*
[4]*School of Automation, Beijing Institute of Technology, Zhong Guan Cun South Street, Haidian District, Beijing 100081, China*
[5]*Changzhou Key Laboratory of Robotics and Intelligent Technology, Changzhou 213022, China*
[6]*Jiangsu Key Laboratory of Special Robots, Hohai University, Changzhou 213022, China*
[7]*College of IoT Engineering, Hohai University, Changzhou 213022, China*

Correspondence should be addressed to Hongbin Ma; mathmhb@ieee.org

Received 20 February 2018; Accepted 3 April 2018; Published 27 June 2018

Academic Editor: Liang Hu

To investigate the effects of muscle fatigue on bioinspired robot learning quality in teaching by demonstration (TbD) tasks, in this work, we propose to first identify the emerging muscle fatigue phenomenon of the human demonstrator by analyzing his/her surface Electromyography (sEMG) recordings and then guide the robot learning curve with this knowledge in mind. The time-varying amplitude and frequency sequences determining the subband sEMG signals have been estimated and their dominant values over short time intervals have been explored as fatigue-indicating features. These features are found carrying muscle fatigue cues of the human demonstrator in the course of robot manipulation. In robot learning tasks requiring multiple demonstrations, the fatiguing status of human demonstrator can be acquired by tracking the changes of the proposed features over time. In order to model data from multiple demonstrations, Gaussian mixture models (GMMs) have been employed. According to the identified muscle fatigue factor, a weight has been assigned to each of the demonstration trials in training stage, which is therefore termed as weighted GMMs (W-GMMs) algorithm. Six groups of data with various fatiguing status, as well as their corresponding weights, are taken as input data to get the adapted W-GMMs parameters. After that, Gaussian mixture regression (GMR) algorithm has been applied to regenerate the movement trajectory for the robot. TbD experiments on Baxter robot with 30 human demonstration trials show that the robot can successfully accomplish the taught task with a generated trajectory much closer to that of the desirable condition where little fatigue exists.

1. Introduction

Muscle fatigue is a complicated phenomenon which is relevant to the functionality of muscles. Generally speaking, it is the decline in ability of a muscle to generate force, which could be a result of excessive exercise. According to the physiological mechanisms causing fatigue, there are two classes of muscle fatigue; among them, neural fatigue is due to the limitations in generating sustained signal by the nerve, while the metabolic fatigue is caused by the falling contraction capacity of muscle fibre. Fatigue limits the sport performance of people. Research found that fatigued muscles produce reduced voluntary force, throwing velocities, and kicking power. Meanwhile, less accuracy and endurance capacity in performing these activities has been reported by Montgomery et al. [1] and Knicker et al. [2]. Pathologists take fatigue assessment as crucial information source of disease progression for diagnosis and treatment. In clinical practice, nowadays qualitative measurements like subjective questionnaires and clinical rating scales are taken as the main protocols of assessing fatigue (Féasson et al. [3] and Mcdonald et al. [4]).

The EMG is a bioelectricity generated by muscle cells. It is known to reflect the activation of neurons controlling muscle contractions. sEMG signals can be collected by attaching surface electrodes on the skin where the target muscle is just beneath. Raw sEMG signals are usually first band filtered to remove noises and retaining the useful information. sEMG related features are characteristics describing the property of the signal in various forms, for example, the amplitude and frequency of the signal, which are computed within a finite time segment of the signal (Wang et al. [5]), the power spectrum (Phinyomark et al. [6]), and so on. Since its noninvasive nature, sEMG has been applied as a research technique to assess muscle recruitment in a variety of scenarios for about three decades. Fatigue generally causes increases in sEMG data, which relates to exercise/sport performance degradation (Carneiro et al. [7] and Beneka et al. [8]). The usefulness of mean frequency (MNF) and median frequency (MDF) of the sEMG signal has been widely investigated in clinical studies and engineering applications (Phinyomark et al. [6] and Mugnosso et al. [9]). To estimate the MNF and MDF of the sEMG signal, a Fourier transform of the autocorrelation of the sEMG signal, that is, the power spectrum or the power spectral density of the sEMG, is first obtained, usually through Periodogram method. The average frequency estimated from the power spectrum is defined as the MNF of the signal. MDF is the frequency that divides the total sum of the sEMG power spectrum into two segments that are equal in amplitude (Oskoei et al. [10]). It has been found that a decreasing MDF over time indicates fatigue (Hollman et al. [11]). Besides these frequency-based features, the other spectral variables which have been employed in sEMG signal analysis include the power spectrum, root mean square values, peak frequency, and the spectral indexes (Farina and Merletti [12] and Phinyomark et al. [6]).

With the advance of robot control strategies under various dynamic scenarios or with even uncertain manipulators, robots nowadays play more proactive roles in coordinating and collaborating with human beings in accomplishing complicated tasks, with skills such as haptic identification (Yang et al. [13]) and human-robot interaction (HRI) (Wolf et al. [14]). Neural interfaces have been introduced for user to control a robot or other intelligent systems through neural commands, such as brain-computer interfaces (BCIs) (Muelling et al. [15] and Yang et al. [16]) or via haptic interaction like teleoperation (Yin et al. [17]). These technologies have been widely employed in complex dynamic scenarios such as robot-assisted surgical operation (Taylor et al. [18]) and disability assistance and rehabilitation (Kaufmann et al. [19]). For tasks requiring physical movements, for example, in manufacturing, sEMG-based neural interface is widely adopted in HRI scenarios (Zucker et al. [20] and Yang et al. [21]). Knowledge and implementation skills transfer by sEMG to telerobot makes it controllable in a remote place and manageable when accomplishing hazardous jobs (Artemiadis and Kyriakopoulos [22], Fukuda et al. [23], and Yang et al. [24]). In our previous studies, sEMG signal has been employed to estimate robot joint stiffness and related muscle tensions (Wang et al. [5]). The sEMG amplitudes from only the very high frequency band have been engaged in impedance and force control, where desirable robot control performance has been achieved. Nowadays, the development of modern controllers has been employed in complex robotic systems, including telerobots. Controller parameters have been estimated to minimize the tracking errors in robot manipulation (Na et al. [25] and Wang et al. [26]). Adaptive methods like unknown input observer and time-varying parameter estimation have also been proposed and applied in complex systems such as vehicle engine system (Na et al. [27]).

TbD is another important HRI research subject. A TbD method is to teach a robot to perform specific tasks through showing the operation by an experienced demonstrator, at once or at multiple times. This flexible way of HRI enables the robot to acquire human-like manipulation skills without complicated steps and at the same time ensures the robot's adaptation to new working conditions (Calinon et al. [28] and Peternel et al. [29]). Nowadays, the taught tasks become more and more complex, for example, carrying on heavy load and obstacles avoidance (Zhang et al. [30]). In these dynamic scenarios, the demonstrator has to conduct multiple demonstrations, where muscle fatigue might occur. Yang et al. have made efforts to remove the tremor's influences on skills transfer when teleoperating a robot (Yang et al. [31]). However, in current TbD research, there has little fatigue-related information been considered. In the field of HRI, fatigue phenomena widely exist, and the challenge of investigating these effects lies in how to inspect and estimate them in dynamic environments. Unlike in clinical studies where fatigue could be measured by subjective ratings, for an engineering application, a systematic method to quantify one's developing fatigue condition over time is essential. On the other hand, the underlying fatigue mechanism is still under research, and their effects in many scenarios are quite subtle to detect, which increases the difficulty of examining them precisely.

In this paper, we present a fatigue-aware robot learning method where the human muscle fatigue issues have been taken into account in the human-robot interaction process. The sEMG data from the human demonstrator have been acquired through a MYO armband worn on the forearm. Fatigue-related parameters have been generated from the collected sEMG recordings thereby. These parameters are derived from the low frequency bands of the sEMG signal where muscle fatigue is generally examined. The instantaneous amplitude and frequency variables which are time-varying sequences of the subband sEMG signal have been estimated. These variables are viewed indicators of the fatiguing status of the demonstrator and are taken into consideration in the robot trajectory learning process. In a complex robot learning application requiring multiple human demonstrations, the detected muscle fatigue status forms the basis of weighing among the different trials. The final learning outcomes will then be generated from the weighted training samples through model adaptation techniques. This work delivers the early efforts of exploring the muscle fatigue effects resulting from real-world HRI tasks, which has brought new perspectives into this research area. With hand-free sEMG measurements, the proposed working

approach will not cause any disturbance to the human operator. Meanwhile, the computational costs required for fatigue scrutiny are manageable in real time as well. With the growing employment of HRI related techniques in a wider social and industrial community nowadays, the efforts made here are expected to inspire more future contributions.

2. Muscle Fatigue Assessment from sEMG

During multiple demonstrations, the human demonstrator will feel tired. It is mainly reflected by the emerging muscle fatigue, which will affect the quality of robot learning. The changes in muscle electricity can describe the underlying muscular activity. As a noninvasive method, sEMG has been taken to measure the muscle fatigue. According to Petrofsky et al. [32], muscle length change causes the amplitude and frequency components of sEMG to vary throughout the duration of fatiguing exercise. This section investigates the intrinsic amplitude and frequency variables in sEMG and how they connect with human muscle fatigue.

For a band-limited signal of a sufficiently small bandwidth, for example, the subband sEMG signal, there is a dominant frequency component assuming the majority of signal power. The amplitude and frequency of this component are viewed as the primary features of the signal. This amplitude-frequency representation is defined as follows (Maragos et al. [33]):

$$\begin{aligned} x(n) &= A(n)\cos[\Theta(n)] + \eta(n) \\ &= A(n)\cos\left[\Omega_c n + \sum_{r=1}^{n} q(r)\right] + \eta(n), \end{aligned} \tag{1}$$

where $A(n)$ and $\Theta(n)$ stand for signal $x(n)$'s amplitude and phase sequence, respectively. The instantaneous frequency is defined as $\Omega(n) = \Theta(n) - \Theta(n-1) = \Omega_c + q(n) = (2\pi/f_s) f_c + q(n)$, where f_s and $q(n)$ denote the sampling frequency (200 Hz) and frequency modulation variable, respectively. $\eta(n)$ delivers any noise and possible errors.

Figure 1 illustrates a segment of sEMG signal and its subbands obtained from band-pass filtering. In each of these subbands, the envelope sequence is estimated and presented by magenta dashed line. Over a short time interval, the mean value of the envelope sequence has been calculated to indicate the dominant amplitude of the subband in green color. Due to the sampling frequency limitation, we choose three-band signal decomposition (<10 Hz, 10–50 Hz, and >50 Hz). We name the average instantaneous amplitude of subband sEMG signal from the three bands as $\mathrm{AIE}_{sb}^{[0,10]}$, $\mathrm{AIE}_{sb}^{[10,50]}$, and $\mathrm{AIE}_{sb}^{[50,100]}$, respectively. The identified parameters in Figure 1 are $\mathrm{AIE}_{sb}^{[0,10]} = 39.55$, $\mathrm{AIE}_{sb}^{[10,50]} = 22.29$, and $\mathrm{AIE}_{sb}^{[50,100]} = 16.81$, respectively. In Figure 2, the instantaneous frequencies of the subband sEMG signals have been tracked, and the principal frequency components are identified as the mean values of the instantaneous frequency sequences over time. Likewise, they have been named as $\mathrm{AIF}_{sb}^{[0,10]}$, $\mathrm{AIF}_{sb}^{[10,50]}$, and $\mathrm{AIF}_{sb}^{[50,100]}$, respectively. The detected dominant frequencies

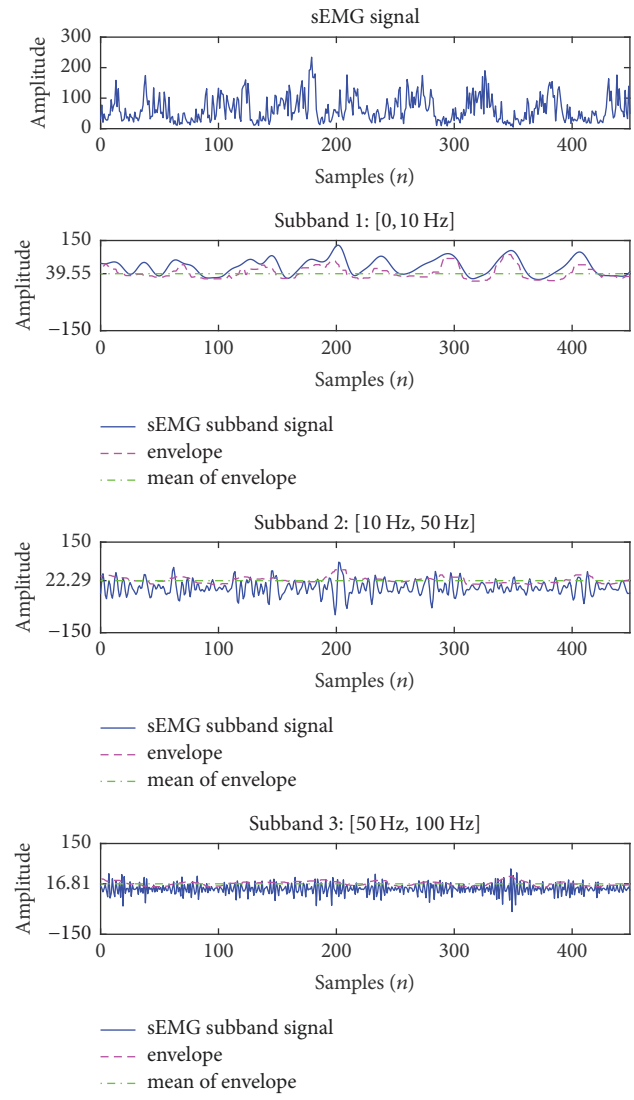

Figure 1: The subband sEMG signals and their envelopes (in magenta dash line). The green dot-dash line in each subband indicates its dominant amplitude.

are 4.57 Hz for band [0, 10 Hz], 31.36 Hz for band [10 Hz, 50 Hz], and 62.95 Hz for band [50 Hz, 100 Hz].

Lower frequency sEMG signals have been found more prominent in identifying muscle fatigue than the higher frequency bands (Petrofsky et al. [32] and Venugopal et al. [34]). The following exploration of fatiguing effects hereby only involves the lower band of sEMG to avoid other irrelevant factors.

3. Robot Movement Representation

Dynamic movement primitive (DMP) is to model the movement streams of a system in discrete time, for example, the trajectory of robot motions (Schaal [35]). DMPs are motion elements or short segments, formed as nonlinear dynamic systems. The robotic joint space can be formulated by multiple DMPs, one per joint state. A DMP system is

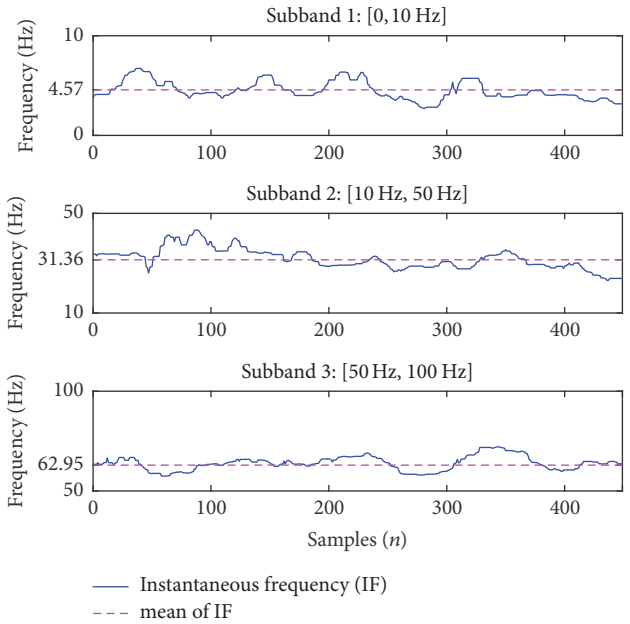

FIGURE 2: The instantaneous and dominant frequencies of subband sEMG signals.

composed of a spring-damper system and an external forcing component, which is defined as follows:

$$\begin{aligned} \tau\dot{\omega} &= k\left(g-\theta\right) - c\omega + \left(g-\theta_0\right) sf\left(s\right), \\ \tau\dot{\theta} &= \omega, \end{aligned} \tag{2}$$

where the variables and constants are explained as follows:

$\theta \in R$: joint angle,

$\omega \in R$: angular velocity of the joint,

$g \in R$: system goal,

$\theta_0 \in R$: start angle,

$\tau > 0$: temporal scaling factor,

$k > 0$: spring constant,

$c > 0$: damping coefficient.

$f : R \to R$ is assumed as a nonlinear continuous bounded function and $s \in R$ is the state of a first-order dynamic system formulated by

$$\tau\dot{s} = -\alpha_s s, \tag{3}$$

where $\alpha_s > 0$ is a time constant and the state s is regarded as a phase variable. This system is referred to as a canonical system. Since it is not dependent on time, the described DMP system in (2) is autonomous, which will finally converge to zero. Empirically, the initial value of s_0 is set to be 1.

DMP is found stable and robust in the presence of external disturbances. It can also adjust the speed of the discrete movement it represents by spatial and temporal scaling.

The original DMP predefines the nonlinear function $f(s)$, which can be expressed as

$$f\left(s\right) = \sum_{i=1}^{N} \gamma_i \phi_i\left(s\right), \tag{4}$$

where $\gamma_i \in R$ are the weights of $\phi_i(s)$ and $\phi_i(s)$ are normalized radial basis functions defined by

$$\phi_i\left(s\right) = \frac{\exp\left(-h_i\left(s-c_i\right)^2\right)}{\sum_{j=1}^{N}\exp\left(-h_j\left(s-c_j\right)^2\right)}, \tag{5}$$

where $c_i > 0$ are the centres and $h_i > 0$ are the widths of the N Gaussian basis functions, with $i = 1, \ldots, N$.

4. Robot Learning from Multiple Human Demonstrations

In order to model data from multiple demonstrations, Gaussian mixture models (GMMs) have been employed. GMMs are a probabilistic model with unknown parameters, consisting of a group of Gaussian distributions.

Each individual demonstration trial produces a set of joint angles of the robot. Therefore, there are N groups of joint angles $\{\theta_{t,i}, \dot{\theta}_{t,i}, \ddot{\theta}_{t,i}\}_{t=0,i=1}^{T_i,N}$ in our data set, where N is the number of demonstration trials. For the ith trial, $\theta_{t,i} \in R$ is the joint angle and T_i is the duration of demonstration. Additionally, the $s_{t,i} \in R$ is the state of system (3) at time step t, and a muscle fatigue factor from the corresponding sEMG data has been calculated as MF_i, where $i = 1, \ldots, N$.

To learn from the data vector set $\{s, f\}$, where f are values of function $f(s)$ in system (2), GMMs have been applied to formulate the joint distribution $P(s, f)$ as described by

$$P\left(s, f\right) = \sum_{k=1}^{K} \alpha_k \mathcal{N}\left(s, f; \mu_k, \Sigma_k\right). \tag{6}$$

Given the dimension d of the input data vector equal to 2, the probability distribution of a Gaussian component $\mathcal{N}(s, f; \mu_k, \Sigma_k)$ is elaborated as follows:

$$\begin{aligned} \mathcal{N}\left(s, f; \mu_k, \Sigma_k\right) &= \frac{e^{-(1/2)([s,f]^T-\mu_k)^T\Sigma_k^{-1}([s,f]^T-\mu_k)}}{(2\pi)^{d/2}\left|\Sigma_k\right|^{1/2}} \\ &= \frac{e^{-(1/2)([s,f]^T-\mu_k)^T\Sigma_k^{-1}([s,f]^T-\mu_k)}}{2\pi\sqrt{\left|\Sigma_k\right|}}. \end{aligned} \tag{7}$$

The GMMs are composed of K Gaussian components here, where the unknown parameters are α_k, μ_k, and Σ_k, with $k = 1, 2, \ldots, K$. $\alpha_k \geq 0$ is the prior probability satisfying $\sum_{k=1}^{K} \alpha_k = 1$, while $\mu_k \in R^{2\times 1}$ and $\Sigma_k \in R^{2\times 2}$ are the mean and covariance

matrix of the kth Gaussian component referred as follows, respectively:

$$\mu_k = \begin{bmatrix} \mu_{s,k} \\ \mu_{f,k} \end{bmatrix}, \quad \Sigma_k = \begin{bmatrix} \Sigma_{s,k} & \Sigma_{sf,k} \\ \Sigma_{fs,k} & \Sigma_{f,k} \end{bmatrix}. \tag{8}$$

These unknown parameters can be retrieved through the Expectation-Maximization (EM) algorithm. We propose to involve weighted Gaussian components rather than the conventional Gaussians in this work in order to take the muscle fatigue effects into account. Considering the fatiguing status during the demonstration phase is varying, the weights across all demonstration data have to vary accordingly. Therefore, compared with the conventional GMMs algorithm, the training data of weighted GMMs (W-GMMs) is scaled by the fatigue factor first. The modified EM algorithm for W-GMMs is elaborated as follows:

(1) Initialization: set initial values of the parameters.

(2) E-step: calculate the response of the kth Gaussian model, $k = 1, 2, \ldots, K$, over the upcoming data points,

$$\widehat{\gamma}_{jk} = \frac{\mathrm{MF}_j \alpha_k \phi\left(x_j \mid \mu_k, \Sigma_k\right)}{\sum_{k=1}^{K} \mathrm{MF}_j \alpha_k \phi\left(x_j \mid \mu_k, \Sigma_k\right)}, \tag{9}$$

where $x_j = \{s_j^T, f_j^T\}$ and MF_j, $j = 1, 2, \ldots, N$ are data vectors and muscle fatigue factor from the jth demonstration, respectively.

(3) M-step: update model parameters by maximum likelihood estimation at new round of iteration to be

$$\widehat{\mu}_k = \frac{\sum_{j=1}^{N} \widehat{\gamma}_{jk} x_j}{\sum_{j=1}^{N} \widehat{\gamma}_{jk}}, \quad \widehat{\Sigma}_k = \frac{\sum_{j=1}^{N} \widehat{\gamma}_{jk} \left(x_j - \mu_k\right)^2}{\sum_{j=1}^{N} \widehat{\gamma}_{jk}}, \quad \widehat{\alpha}_k = \frac{\sum_{j=1}^{N} \widehat{\gamma}_{jk}}{N}. \tag{10}$$

(4) Repeat the E-step and M-step until convergence.

The $\widehat{f}$ function can be estimated through Gaussian mixture regression (GMR) algorithm. In GMR, the conditional probability $P(f \mid s)$ is elaborated by

$$P\left(f \mid s\right) \sim \sum_{k=1}^{K} \beta_k \mathcal{N}\left(\widehat{\eta}_k, \widehat{\sigma}_k^2\right), \tag{11}$$

Figure 3: The Baxter robot.

where

$$\widehat{\eta}_k = \mu_{f,k} + \Sigma_{fs,k} \left(\Sigma_{s,k}\right)^{-1} \left(s - \mu_{s,k}\right), \quad \widehat{\sigma}_k^2 = \Sigma_{f,k} - \Sigma_{fs,k} \left(\Sigma_{s,k}\right)^{-1} \Sigma_{sf,k}, \quad \beta_k = \frac{\alpha_k \mathcal{N}\left(s; \mu_{s,k}, \Sigma_{s,k}\right)}{\sum_{i=1}^{K} \alpha_i \mathcal{N}\left(s; \mu_{s,i}, \Sigma_{s,i}\right)}. \tag{12}$$

According to the linear transformation property of Gaussian distributions, $P(f \mid s)$ can be approximated as $P(f \mid s) \sim \mathcal{N}(\widehat{\eta}, \widehat{\sigma}^2)$, with $\widehat{\eta} = \sum_{k=1}^{K} \beta_k \widehat{\eta}_k$ and $\widehat{\sigma}^2 = \sum_{k=1}^{K} \beta_k^2 \widehat{\sigma}_k^2$, where $\widehat{\eta}$ is the expectation.

Finally, the nonlinear function $f(s)$ is estimated by

$$\widehat{f}\left(s\right) = \widehat{\eta} = \sum_{k=1}^{K} \beta_k \left(\mu_{f,k} + \Sigma_{fs,k} \left(\Sigma_{s,k}\right)^{-1} \left(s - \mu_{s,k}\right)\right), \tag{13}$$

where $\widehat{f}(s)$ is bounded since $\beta_k \in [0, 1]$ and $s \in (0, 1]$.

5. Experiments

In this section, we setup our experimental platform and verify the proposed method by a robot teaching by demonstration experiment which consists of a demonstration phase, a learning phase, and a reproduction phase.

5.1. Platform Setup. The Baxter robot has been employed to verify the proposed method. Baxter is a semihumanoid industrial robot developed by Rethink Robotics, whose head is of 2-DOF and the two arms are of 7-DOF (shoulder joint: $S0$ and $S1$; elbow joint: $E0$ and $E1$; wrist joint: $W1$, $W2$, and $W3$). Figure 3 gives us a picture of the Baxter robot. Besides industrial usage, it has been employed in HRI and human-robot collaboration (HRC) research widely (Reddivari et al. [36]). In the experiment, the human demonstrator will drag the end effector of the robot to complete a demonstration task, during which the robot joint angles will be recorded.

Figure 4 shows the way of sEMG data collection in the experiments. During the manipulation, MYO armband is worn on the arm of the demonstrator to record the sEMG signals generated, where the movement of human arm is mainly driven by biceps brachii. The MYO armband is composed of 8 sEMG electrodes and a 9-axis inertial

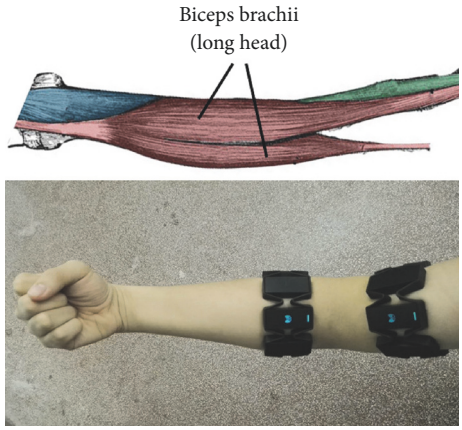

Figure 4: Demonstrator wearing the MYO armband.

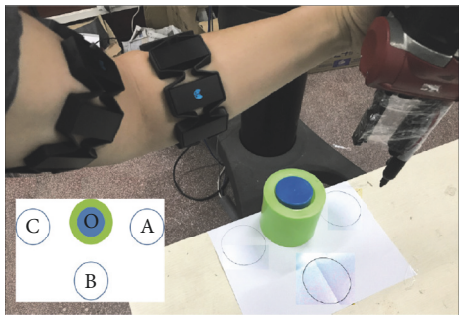

Figure 5: A scene captured in the experiment.

measurement unit. These electrodes capture the bioelectricity changes of the arm muscle of the human subject who wears it. The default sampling frequency of sEMG signal acquisition is 200 Hz. The acquired sEMG recordings are transmitted to the client computer through Bluetooth.

5.2. Demonstration Phase. As shown in Figure 5, there is a pen fixed at the end effector of the Baxter robot. The rest place of the pen is on the top of the obstacle (the stacked cylinder). Dragged by the human demonstrator, the robot will complete the following action: at first, the pen at the end effector pokes the first circle (A); it then bypasses the obstacle and pokes the second circle (B); and then it bypasses the obstacle again and pokes the third circle (C), and finally it returns to its rest place. In this way, the passing path of the pen is A → O → B → O → C → O.

This demonstration is repeated 30 times. In the course of each demonstration, the joint angles of the robot and the sEMG signals of the human demonstrator are recorded. Although the passing path is fixed, the trajectory of robot motion and the duration of teaching in each trial vary. However, all trajectories share the exact same starting and end places.

5.3. Learning Phase and Reproduction Phase. The sEMG data for fatigue investigation in this task is from the sensors

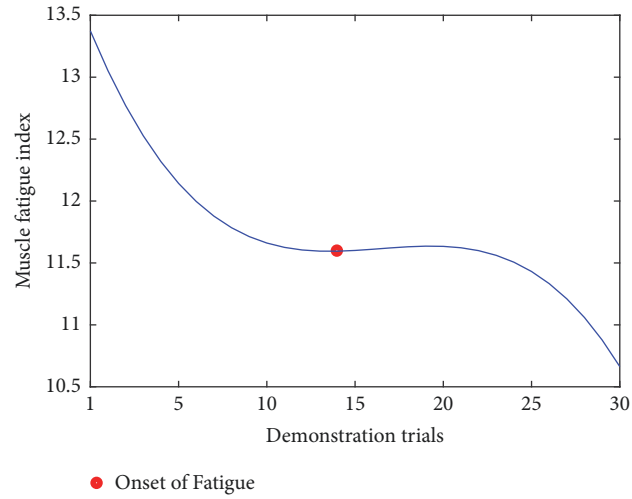

Figure 6: The smoothed curve of the proposed fatigue-related features (average instantaneous amplitude of sEMG signal) across all trials during the human demonstration to robot.

attached to the biceps brachii, since the movement of human arm is mainly driven by it. As described in Section 2, we extract the instantaneous amplitude sequence of sEMG subband [0, 10 Hz] captured by the second channel of MYO armband and compute the mean values of that time-varying sequence at every 2 s time interval to acquire the fatigue parameters across all 30 demonstrations. To reveal the most significant trend and remove fluctuations, a 3rd-order polynomial function has been used to fit the data samples $AIE_{sb}^{[0,10]}$. Figure 6 shows the smoothed data samples over all 30 trials after curve fitting. We define an Onset of Fatigue (OF) index as the flex point of the cubic function in the figure. When training W-GMMs, six groups of data have been chosen to learn the new robot trajectory; three of them are from demonstrations before the OF, while the others are from trails after the OF. Their muscle fatigue factors are taken as weights in the W-GMMs training process, which are calculated and normalized to be 0.9, 0.8, 0.7, 0.4, 0.3, and 0.2, respectively.

Both the duration and the data amount recorded in each demonstration vary from one to another. In Figure 7(a), we randomly select three samples of data to observe, which are the angles of shoulder joint *S*0. It is found that they are different in duration and misaligned in time. Dynamic Time Warping (DTW) algorithm is therefore applied to align the data along the timeline. Figure 7(b) shows the aligned data after the DTW processing.

As mentioned, six groups of data, including three before the OF, and three after that, as well as their corresponding weights are taken as training data to build the W-GMMs. Figure 8 illustrates the learning process of the W-GMMs. Figure 8(a) shows the training data samples in the joint space. Figure 8(b) reveals the GMMs after training, which encodes the joint distribution with sixteen Gaussian components. Figure 8(c) demonstrates the learning results from W-GMMs, with the training samples depicted in dotted lines. It is

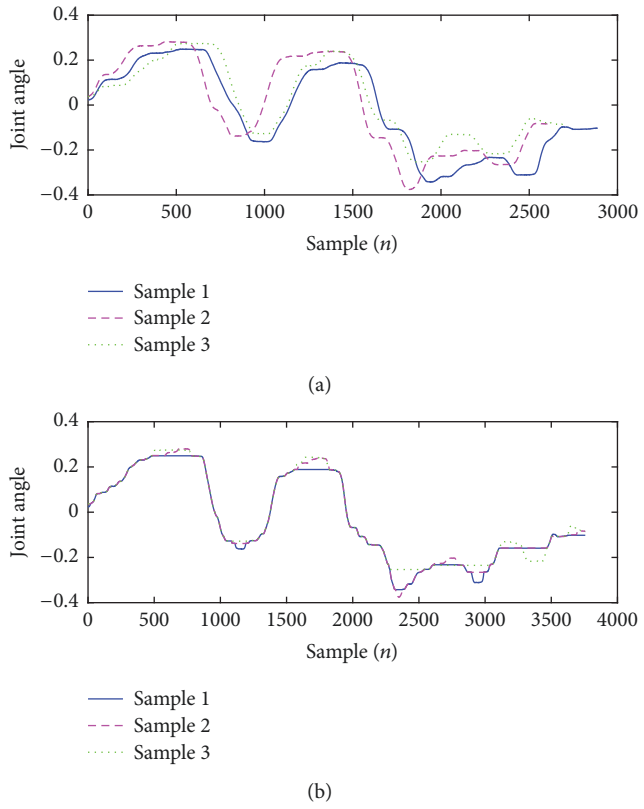

FIGURE 7: (a) Three original samples of the joint angle $S0$. (b) The processed samples after DTW time alignment.

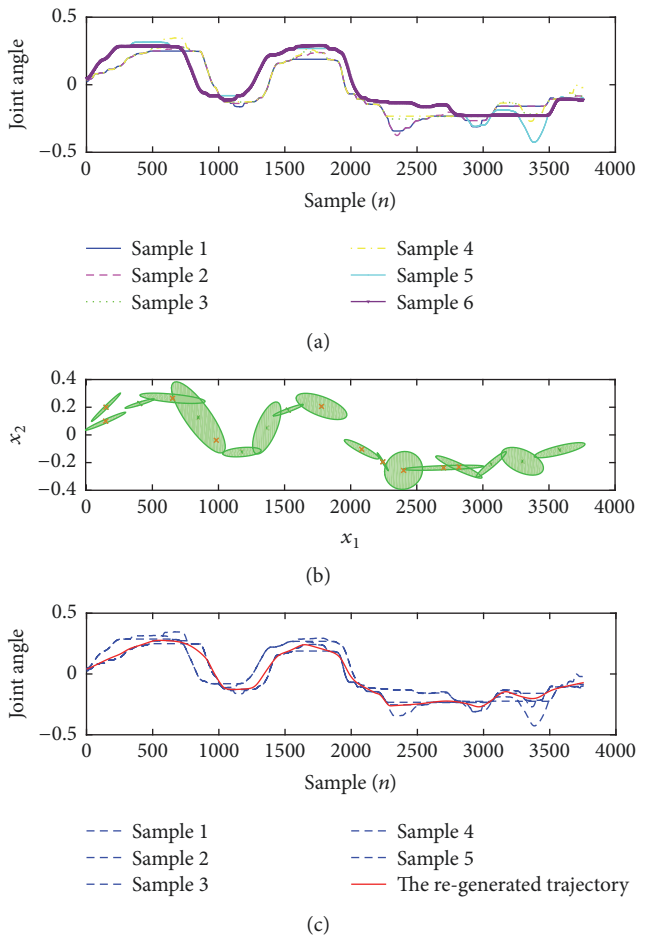

FIGURE 8: The learning process of the W-GMMs. (a) Training data samples in the joint space $S0$. (b) Gaussian mixture components formed by the training data. (c) Regenerated (learned) trajectory from the W-GMMs.

observed that, by involving the fatigue-related weights in GMMs training, the training data with larger weights counts more in the training results, which means in this way the demonstrations when less fatigue occur are more influential in robot learning outcomes.

Angle data of all seven joints, including two shoulder joints $S0$ and $S1$, two elbow joints $E0$ and $E1$, and three wrist joints $W1$, $W2$, and $W3$, have been taken into account in the robot learning experiment. Figure 9 illustrates the learning results for each joint from the W-GMMs. The Baxter robot then successfully accomplishes the taught task by the human demonstrator after receiving these learned joint angle data. Figure 10 demonstrates the trajectory of the Baxter end effector in Cartesian space when accomplishing the task.

6. Conclusion

Robot learning manipulation skills from human demonstration is a straightforward yet effective way of knowledge transfer. However, the manipulation, especially for complex tasks with heavy loads, will make the human demonstrator feel tired. The purpose of this study is to inspect the influences of muscle fatigue on robot learning from human demonstration. We propose new fatigue-indicating sEMG features, which have been explored from analyzing the varying amplitude and frequency components within the sEMG during biceps brachii muscle contractions. These newly presented features have been employed to identify the fatigue onset in the process of a fatiguing TbD task, which has been further taken to guide the learning curve of the robot. A weighted GMM has been employed to learn the robot joints angle from data of multiple demonstration trials, where the muscle fatigue factors identified in each of these trials have been considered. In this way, the regenerated movement trajectory shows its closeness with the ideal condition when less fatigue detected. In the TbD experiments carried out, the Baxter robot successfully completes the task taught by the human demonstrator with desirable performance. This work describes the efforts on investigating the muscle fatigue effects under the environments of HRI manipulation. With growing interests and needs of applying HRI techniques in various working conditions, it is expected that the efforts made here would bring new perspectives into relevant research areas.

Conflicts of Interest

The authors declare that they have no conflicts of interest.

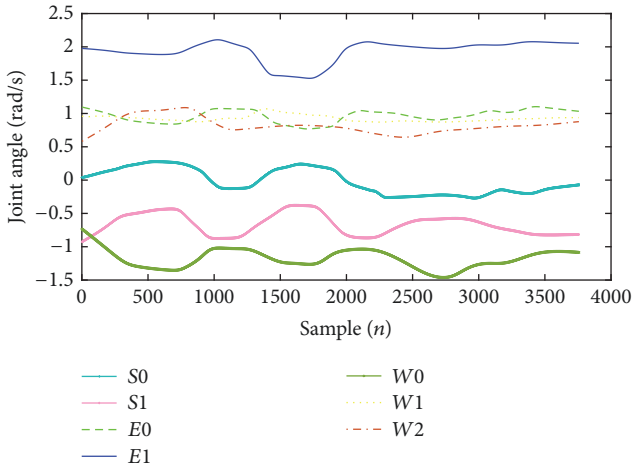

Figure 9: The seven joint angles of the Baxter robot right arm.

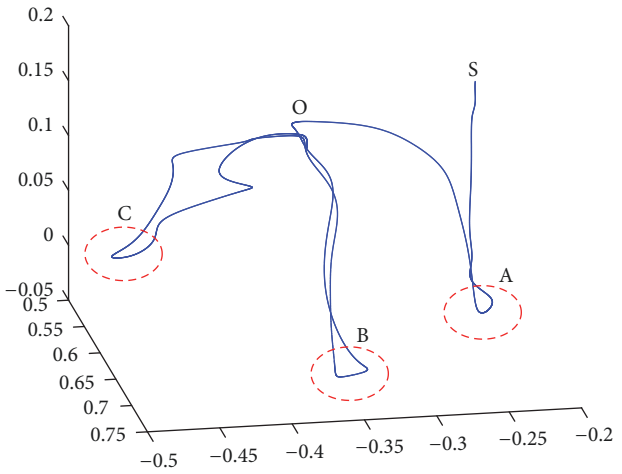

Figure 10: The trajectory of the Baxter robot right arm when accomplishing the learned task.

Acknowledgments

This research was partially supported by Natural Science Foundation of Beijing under Grant no. 17D30118, the National Natural Science Foundation of China under Grants no. 61332010, no. 61473038, and no. 91648117, the Fundamental Research Funds for the Key Research and Development Program of Jiangsu under Grants BE2017071 and BE2017647, the Projects of International Cooperation and Exchanges of Changzhou under Grant CZ20170018, and the European Union Seventh Framework Programme (FP7/2007–2013) under Grant 288899.

References

[1] P. G. Montgomery, D. B. Pyne, W. G. Hopkins, J. C. Dorman, K. K. Cook, and C. L. Minahan, "The effect of recovery strategies on physical performance and cumulative fatigue in competitive basketball," *Journal of Sports Sciences*, vol. 26, no. 11, pp. 1135–1145, 2008.

[2] A. J. Knicker, I. Renshaw, A. R. H. Oldham, and S. P. Cairns, "Interactive processes link the multiple symptoms of fatigue in sport competition," *Sports Medicine*, vol. 41, no. 4, pp. 307–328, 2011.

[3] L. Féasson, J. Camdessanché, L. El Mhandi, P. Calmels, and G. Millet, "Fatigue and neuromuscular diseases," *Annales de Réadaptation et de Médecine Physique*, vol. 49, no. 6, pp. 375–384, 2006.

[4] C. M. Mcdonald, E. K. Henricson, J. J. Han et al., "The 6-minute walk test in Duchenne/Becker muscular dystrophy: Longitudinal observations," *Muscle & Nerve*, vol. 42, no. 6, pp. 966–974, 2010.

[5] N. Wang, C. Yang, M. R. Lyu, and Z. Li, "An EMG enhanced impedance and force control framework for telerobot operation in space," in *Proceedings of the IEEE Aerospace Conference*, pp. 1–10, Big Sky, Mont, USA, March 2014.

[6] A. Phinyomark, S. Thongpanja, H. Hu, P. Phukpattaranont, and C. Limsakul, "Computational intelligence in Electromyography analysis - A perspective on current applications and future challenges," in *The Usefulness of Mean And Median Frequencies in Electromyography Analysis*, pp. 195–220, Intech Open, 2012.

[7] J. G. Carneiro, E. M. Gonçalves, T. V. Camata et al., "Influence of gender on the EMG signal of the quadriceps femoris muscles and performance in high-intensity short-term exercise," *Electroencephalography and Clinical Neurophysiology*, vol. 50, no. 7-8, pp. 326–332, 2010.

[8] A. G. Beneka, P. K. Malliou, V. Missailidou et al., "Muscle performance following an acute bout of plyometric training combined with low or high intensity weight exercise," *Journal of Sports Sciences*, vol. 31, no. 3, pp. 335–343, 2013.

[9] M. Mugnosso, F. Marini, M. Gillardo, P. Morasso, and J. Zenzeri, "A novel method for muscle fatigue assessment during robot-based tracking tasks," in *Proceedings of the 2017 International Conference on Rehabilitation Robotics, ICORR 2017*, pp. 84–89, gbr, July 2017.

[10] M. A. Oskoei, H. Hu, and J. Q. Gan, "Manifestation of fatigue in myoelectric signals of dynamic contractions produced during playing PC games," in *Proceedings of the 30th Annual International Conference of the IEEE Engineering in Medicine and Biology Society, EMBS'08*, pp. 315–318, can, August 2008.

[11] J. H. Hollman, J. M. Hohl, J. L. Kraft, J. D. Strauss, and K. J. Traver, "Does the fast Fourier transformation window length affect the slope of an electromyogram's median frequency plot during a fatiguing isometric contraction?" *Gait & Posture*, vol. 38, no. 1, pp. 161–164, 2013.

[12] D. Farina and R. Merletti, "Comparison of algorithms for estimation of EMG variables during voluntary isometric contractions," *Journal of Electromyography & Kinesiology*, vol. 10, no. 5, pp. 337–349, 2000.

[13] C. Yang, K. Huang, H. Cheng, Y. Li, and C. Su, "Haptic identification by ELM-controlled uncertain manipulator," *IEEE Transactions on Systems, Man, and Cybernetics: Systems*, vol. 470, no. 8, pp. 2398–2409, 2017.

[14] S. Wolf, T. Bahls, M. Chalon et al., "Soft Robotics - Transferring Theory to Application, chapter Soft Robotics with Variable Stiffness Actuators: Tough Robots for Soft Human Robot Interaction," in *Soft Robotics - Transferring Theory to Application*, A. Albu-Schäffer, Ed., pp. 231–254, Springer-Verlag, Berlin, Germany, 2015.

[15] K. Muelling, A. Venkatraman, J.-S. Valois et al., "Autonomy infused teleoperation with application to brain computer interface controlled manipulation," *Autonomous Robots*, vol. 41, no. 6, pp. 1401–1422, 2017.

[16] C. Yang, H. Wu, Z. Li, W. He, N. Wang, and C. Su, "Mind Control of A Robotic Arm with Visual Fusion Technology," *IEEE Transactions on Industrial Informatics*, 2017.

[17] X. Yin, S. Guo, H. Hirata, and H. Ishihara, "Design and experimental evaluation of a teleoperated haptic robot-assisted catheter operating system," *Journal of Intelligent Material Systems and Structures*, vol. 27, no. 1, pp. 3–16, 2016.

[18] R. H. Taylor, A. Menciassi, G. Fichtinger, P. Fiorini, and P. Dario, "Handbook of Robotics, chapter Medical Robotics and Computer-Integrated Surgery," in *Springer Handbook of Robotics*, Springer, 2016.

[19] T. Kaufmann, A. Herweg, and A. Kübler, "Toward brain-computer interface based wheelchair control utilizing tactually-evoked event-related potentials," *Journal of NeuroEngineering and Rehabilitation*, vol. 11, no. 1, article 7, 2014.

[20] M. Zucker, S. Joo, M. X. Grey et al., "A General-purpose System for Teleoperation of the DRC-HUBO Humanoid Robot," *Journal of Field Robotics*, vol. 32, no. 3, pp. 336–351, 2015.

[21] C. Yang, C. Zeng, P. Liang, Z. Li, R. Li, and C.-Y. Su, "Interface Design of a Physical Human-Robot Interaction System for Human Impedance Adaptive Skill Transfer," *IEEE Transactions on Automation Science and Engineering*, 2017.

[22] P. K. Artemiadis and K. J. Kyriakopoulos, "EMG-based control of a robot arm using low-dimensional embeddings," *IEEE Transactions on Robotics*, vol. 26, no. 2, pp. 393–398, 2010.

[23] O. Fukuda, T. Tsuji, M. Kaneko, and A. Otsuka, "A human-assisting manipulator teleoperated by EMG signals and arm motions," *IEEE Transactions on Robotics and Automation*, vol. 19, no. 2, pp. 210–222, 2003.

[24] C. Yang, X. Wang, Z. Li, Y. Li, and C. Su, "Teleoperation control based on combination of wave variable and neural networks," *IEEE Transactions on Systems, Man, and Cybernetics: Systems*, 2017.

[25] J. Na, M. N. Mahyuddin, G. Herrmann, X. Ren, and P. Barber, "Robust adaptive finite-time parameter estimation and control for robotic systems," *International Journal of Robust and Nonlinear Control*, vol. 25, no. 16, pp. 3045–3071, 2015.

[26] S. Wang, X. Ren, J. Na, and T. Zeng, "Extended-state-observer-based funnel control for nonlinear servomechanisms with prescribed tracking performance," *IEEE Transactions on Automation Science and Engineering*, vol. 14, no. 1, pp. 98–108, 2017.

[27] J. Na, A. S. Chen, G. Herrmann, R. Burke, and C. Brace, "Vehicle Engine Torque Estimation via Unknown Input Observer and Adaptive Parameter Estimation," *IEEE Transactions on Vehicular Technology*, 2017.

[28] S. Calinon, D. Bruno, M. S. Malekzadeh, T. Nanayakkara, and D. G. Caldwell, "Human-robot skills transfer interfaces for a flexible surgical robot," *Computer Methods and Programs in Biomedicine*, vol. 116, no. 2, pp. 81–96, 2014.

[29] L. Peternel, T. Petrič, E. Oztop, and J. Babič, "Teaching robots to cooperate with humans in dynamic manipulation tasks based on multi-modal human-in-the-loop approach," *Autonomous Robots*, vol. 36, no. 1-2, pp. 123–136, 2014.

[30] H. Zhang, X. Han, M. Fu, and W. Zhou, "Robot Obstacle Avoidance Learning Based on Mixture Models," *Journal of Robotics*, vol. 2016, Article ID 7840580, 2016.

[31] C. Yang, J. Luo, Y. Pan, Z. Liu, and C. Su, "Personalized variable gain control with tremor attenuation for robot teleoperation," *IEEE Transactions on Systems, Man, and Cybernetics: Systems*, pp. 1–12, 2017.

[32] J. S. Petrofsky, R. M. Glaser, and C. A. Phillips, "Evaluation of the amplitude aud frequency components of the surface emg as an index of muscle fatigue," *Ergonomics*, vol. 25, no. 3, pp. 213–223, 1982.

[33] P. Maragos, J. F. Kaiser, and T. F. Quatieri, "Energy separation in signal modulations with application to speech analysis," *IEEE Transactions on Signal Processing*, vol. 41, no. 10, pp. 3024–3051, 1993.

[34] G. Venugopal, M. Navaneethakrishna, and S. Ramakrishnan, "Extraction and analysis of multiple time window features associated with muscle fatigue conditions using sEMG signals," *Expert Systems with Applications*, vol. 41, no. 6, pp. 2652–2659, 2014.

[35] S. Schaal, "Dynamic Movement Primitives -A Framework for Motor Control in Humans and Humanoid Robotics," in *Adaptive Motion of Animals and Machines*, Springer, Tokyo, Japan, 2006.

[36] H. Reddivari, C. Yang, Z. Ju, P. Liang, Z. Li, and B. Xu, "Teleoperation control of Baxter robot using body motion tracking," in *Proceedings of the International Conference on Multisensor Fusion and Information Integration for Intelligent Systems (MFI '14)*, pp. 1–6, Beijing, China, September 2014.